CrystEngComm

Accepted Manuscript

ROYAL SOCIETY OF CHEMISTRY

www.rsc.org/crystengcomm

HRTEM study on the ordered phases in $Hg_3In_2Te_6$ crystals grown by Bridgman method

Lin Luo, Wanqi Jie*, Yadong Xu, Yihui He, Lingyan Xu, Li Fu

State Key Laboratory of Solidification Processing, School of Materials Science and Engineering, Northwestern Polytechnical University, Xi'an 710072, China

Abstract:

High-resolution transmission electron microscopy (HRTEM) is used to investigate $Hg_3In_2Te_6$ (MIT) crystals grown by Bridgman method. The results show that at least two new ordered phases exist in the crystals. Their corresponding superstructure spots 1/3{422} and 1/6{422} are observed for the first time in defect zinc-blende crystals. The possible structural models of the two ordered phases are suggested based on HRTEM images. A mechanism is proposed to explain the formation and evolution of the two ordered phases. It is thought that the disorder-order phase transformation was not absolutely prevented during furnace cooling process, due to the small cooling rate and the low thermal conductivity of the defect zinc-blende materials.

Keywords: semiconductors; structural vacancy; disorder-order transformation; high resolution transmission electron microscopy (HRTEM); superstructure.

* Corresponding author at: 127 Youyi Xilu, Xi'an 710072, China. Tel.: +862988486065; fax: +862988495414. E-mail address:jwq@nwpu.edu.cn

1. Introduction

In $Hg_3In_2Te_6$ (MIT) crystals, one-sixth of the cation sublattice sites are structural vacancies (about 10^{21} cm^{-3}) due to the difference in valence between Hg and In [1]. MIT crystallizes into the disordered defect zinc-blende phase at high temperature, in which structural vacancies are distributed randomly in the cation sublattice. The disordered phase is transformed into several ordered phases at 290 degree Celsius, where the arrangements of structural vacancies are fully or partially ordered [2-4].

MIT is regarded as a promising novel photoelectric compound for fiber-optic communication [5]. One of the key reasons is that its room-temperature band-gap energy (0.72eV) is matched with the most common transmission signal wavelength 1.55μm for long-distance fiber-optic communication [6]. Generally, band-gap energy has a one-to-one correspondence with alloy composition [7]. Therefore, it can be considered that ordered MIT phases and the disordered MIT phase have the same band-gap energy. The detectors used in fiber-optic communication should have fast response speeds and low noises, which demand that MIT crystals possess high carrier mobility and low dislocation density. It is well known that low thermal conductivity gives rise to high thermal stress inside the ingots and increases dislocation density. Hence, the crystals should have high thermal conductivity to grow crystals with low dislocation density from the melt, such as Bridgman method. In comparison with ordered phases, the disordered phase usually has higher carrier mobility and thermal conductivity [8, 9]. Therefore, MIT crystals with the disordered phase are expected, and on the contrary the ordered phases are expected to be avoided.

To achieve the goal, ingots are usually cooled from high temperature to low temperature by

furnace cooling, to avoid disorder-order phase transformation. The goal was considered to be realized in many papers [10-16], due to the absence of superlattice peaks in X-ray diffraction (XRD) patterns. However, since the detection limit in volume of powder XRD is 5%, the existence of MIT ordered phases cannot be ruled out.

In this paper, we carry out HRTEM observations to study MIT samples. The results show that MIT ingots contain at least two types of ordered phases, which confirms the existence of disorder-order phase transformation. The corresponding superstructure spots of the two ordered phases are 1/3{422} and 1/6{422}. To our knowledge, 1/3{422} and 1/6{422} have not been reported in defect zinc-blende materials before. We suggest two possible structural models of the two ordered phases based on HRTEM images. Finally, we propose a mechanism to explain the formation and evolution of the two ordered phases.

2. Material and methods

All MIT samples used in the experiments came from ingots grown by vertical Bridgman method in the State Key Laboratory of Solidification Processing (SKLSP) in China. The ingots were cooled from 360 degree Celsius to room temperature by furnace cooling after crystal growth and in-situ annealing.

A portion of the samples were cleaned and finely ground into powders for XRD analysis. The X'Pert MPO Pro X-ray diffractometer was used to collect XRD data in 2θ range of 10~80°. The X-ray source was $Cu_{K\alpha}$ with the wavelength of 0.15406nm. The accelerating voltage and current were 40 kV and 35 mA, respectively.

The other portions of the samples were prepared for TEM analysis. The wafers were mechanically ground to 40 μm thickness, and then thinned using Gatan 691 ion beam thinner to

obtain electron transparent thin areas. Small angle, low voltage and liquid nitrogen cooling were used to avoid the artifacts during milling. HRTEM were performed using a Tecnai F30 G^2 electron microscope with the incident electron energy of 300 keV. Simulation of HRTEM images was performed by using a multislice approach. The simulation conditions are given in the Supporting Information.

3. Results

A typical powder XRD pattern of MIT samples measured at room temperature is shown in Fig. 1a. The analysis shows that the samples are pure disordered MIT phases (PDF number: 65-5765, $F\bar{4}3m$) and no superlattice peaks are found, which is the same as that reported in previous papers [10-15]. Seemingly, the samples do not contain ordered phases.

However, considering that the detection limit of XRD measurements (concentration > 5%), the existence of ordered MIT phases still cannot be ruled out. Therefore, HRTEM observations with higher accuracy were carried out. Fig. 1b is a typical HRTEM image observed in most areas of TEM samples. A fast Fourier transform (FFT) image of Fig. 1b is shown in Fig. 1c. HRTEM and FFT images are indexed as the disordered MIT phase.

Nevertheless, a different HRTEM image was found in a few areas of TEM samples, as shown in Fig. 2a. Comparing with Fig. 1b, white dots with triple periodicities in <422> directions can be identified. To better illustrate the new periodic arrangement, an FFT image of Fig. 2a is produced as shown in Fig. 2b. Its corresponding schematic diagram is shown in Fig. 2c. According to the relative intensity, the diffraction spots in FFT image can be divided into two sets. The set of diffraction spots (basic spot) with strong intensity, as marked by white circles, is indexed as the fundamental reflections corresponding to the disordered MIT phase. The weak set (spot 1) exists

at 1/3 and 2/3 positions between two neighboring basic spots along <422> directions, which is consistent with the extra periodic arrangements in Fig. 2a. The positions are forbidden in the diffraction patterns of the zinc-blende structure, so spot 1 is ascribed to a superstructure.

For defect zinc-blende materials [3, 8, 9, 17-21], such as Ga_2Te_3, In_2Te_3 and $Cu_2Ga_4Te_7$, periodically arranged bright and dark dots of HRTEM images and superstructure spots are usually ascribed to the periodic arrangement of structural vacancies on the cation sublattice. Researchers in the field of defect zinc-blende materials did not take into account possible ordering of cations. Hence, Fig. 2 shows that TEM samples contain an ordered phase. For convenience, the ordered phase with 3×3×3 superstructure [2] and the ordered phase corresponding to spot 1 are named as α and β ordered phases, respectively.

For further comparison, we measured the interplanar distances along three <422> directions. The results are shown in Tab. 1. D_1 is 2.92 times of $d_{(422)}$, which suggests the lattice constant of β phase becomes smaller after ordering of vacancies. In order to confirm this result, SAED pattern of β phase along [$\bar{1}11$] zone axis is recorded as shown in Fig. 3. The set of diffraction spots with strong intensity is corresponding to the disordered phase. The weak set indicated by the red circles is the diffraction spots of β phase. The interplanar distance (0.371nm) of Spot A is 2.83 times of $d_{(422)}$ (0.131nm) measured in Fig. 3. Moreover, the inset of Fig. 3 shows that the interplanar distance of β phase in the regions marked by arrows is also smaller than that of the disordered phase along [200] direction. The deviations in the interplanar distances suggest that 1/3{422} spots and HRTEM patterns of β phase really reflect structural features.

Besides, another HRTEM image can also be observed in a few areas of TEM samples. As shown in Fig. 3a, white dots possess six fold periodicities in <422> directions. An FFT image of

Fig. 4a and its corresponding sketch map are shown in Fig. 4b and 4c, respectively. There is another set of forbidden diffraction spots (spot 2) existed at the positions dividing the interval between two neighboring basic spots into six equal parts along <422> directions, which is consistent with the six fold periodicities in Fig. 4a. The ordered phase corresponding to spot 2 is named as γ ordered phase. It should be stressed that, γ phase is harder to be observed than β phase. A typical EDX result (Fig. S1 in the Supporting Information), which is obtained in the areas where the two HRTEM images are recorded, points out that the composition is consistent with $Hg_3In_2Te_6$.

The content of γ phase is very low. This is because that γ phase is an unstable transition phase indicated by analyses in section 4.3. Hence, the superstructure spots (1/6{422}) of γ phase is hard to be observed in SAED patterns. However, Tab. 1 shows D_2 is 5.67 times of $d_{(422)}$, which indicates that the diffraction spots of γ phase do not coincide with that of the disordered phase in some regions, if the spots can be seen in the SAED patterns. Therefore, it is suggested that 1/6{422} spots and HRTEM patterns of γ phase also really reflect structural features and they are not caused by multiple scattering.

In the next step, we will focus on the specific arrangement of structural vacancies in β and γ phases. Comparison of the HRTEM images gives the sketch maps of Fig. 2a and 4a, as shown in Fig. 2d and Fig. 4d, respectively. Their ordered units are Fig. 2e and Fig. 4e, respectively. Fig. 2d shows that one of every three <110> atom arrays are occupied entirely by ordered structural vacancies. For Fig. 4d, one of every six <110> atom arrays contain ordered structural vacancies. In the <110> array, one of every two positions are occupied by ordered structural vacancies.

4. Discussion

4.1 Formation reason of ordered phases

The above results show that TEM samples contain at least two types of ordered phases. The superstructure spots can also be found in powder TEM samples prepared by cleavage method. The finding suggests that MIT ingots contain two or more ordered phases, appearing as small islands embedded in the disordered phase, although superstructure diffraction peaks cannot be revealed in powder XRD spectra.

Theoretically, disorder-order phase transformation can be prevented through rapid cooling. However, part of the MIT ingots stay at phase transformation temperature for a relative long period, since its thermal conductivity is as small as 8.8 $mW \cdot cm^{-1} \cdot K^{-1}$ [22], only 4% of thermal conductivity of Si (210 $mW \cdot cm^{-1} \cdot K^{-1}$) [23], and practical cooling rate of furnace cooling is not fast enough. Consequently, a portion of the ingots are transformed into ordered phases. If a faster cooling is used, phase transformation could be prevented. Nevertheless, thermal stress within the crystals will be increased, which causes high dislocation density, poor crystal quality and even cracks.

In general, defect zinc-blende materials have low thermal conductivity, owing to strong phonon-vacancy scattering [8, 24]. Thus, the formation of ordered phases is hard to be avoided absolutely in the ingots with defect zinc-blende structure. The result suggests that the influence of ordered phases should be taken into account as second-phases in other materials [25-28], when physical properties and device performances of the crystals are analyzed.

4.2 Structural models of β and γ phases

To our knowledge, for the common defect zinc-blende materials, such as In_2Te_3 [9, 29], Ga_2Te_3 [8, 17, 20], Ga_2Se_3 [18] and Ga_2S_3 [30, 31], the following superstructure spots have been reported: 1/3{111} [9], 1/10{111} [8, 17, 19], 1/2{111} [32], 1/3{220} [32-36], 1/3{200} [37]. For MIT, only a set of superstructure spot 1/3{220} has been reported in previous work [3]. For other FCC materials, 1/3{422} is mainly found in Au [38-40] and Ag [41, 42] plate-like nanocrystals. Therefore, it can be concluded that superstructure spots 1/3{422} and 1/6{422} have not been reported in defect zinc-blende crystals.

In the following analysis, the possible structural model of β phase will be given based on Fig. 2. The stacking sequence of the zinc-blende structures along <111> direction is ABCABC.... Ordered structural vacancies (blue dots) in Fig. 2d are postulated to be located at an A layer. For distinction, A layers with and without ordered structural vacancies are denoted by V and A layers, respectively. Atoms (Hg, In and disordered structural vacancies) in V and A layers are expressed by green dots. Atoms in B and C layers are represented by yellow and red dots, respectively. Consequently, the ordered unit of β phase in Fig. 2d can be expressed by Fig. 5a.

For constructing the structural model of β phase, $(\bar{1}11)$ plane and $[\bar{1}11]$ direction of the disordered phase are treated as a-b plane and c axis of β phase, respectively. Nevertheless, the number (n) of atom layers along c axis is still unknown. First, if every three $(\bar{1}11)$ atom layers contain one V layer, stacking sequence will be VBCVBC... and the proportion p of ordered structural vacancies in cation sublattice will be 1/3, which will exceed the nominal proportion p_0 of structural vacancies, i.e. 1/6. Secondly, supposing that every six $(\bar{1}11)$ atom layers contain one V layer, stacking sequence will be VBCABCVBCABC... and p will be equal to p_0. Thus, the possible structural model of β phase shown in Fig. 5b is presented by the space group P3m1 with lattice parameters $a_\beta = b_\beta = \sqrt{2}a/2$, $c_\beta = 2\sqrt{3}a$, $\alpha_\beta = \beta_\beta = 90°$, $\gamma_\beta = 120°$, where *a* is the

lattice constant (0.6298nm) of the disordered phase. It should be noticed that the structural vacancies in β phase are entirely ordered.

Fig. 5c and Fig. 5d are a simulated electron diffraction pattern and a HRTEM image along $[\bar{1}11]$ zone axis, which are consistent with the experimental FFT image (Fig. 2b) and HRTEM image (Fig. 2a), respectively. Fig. 5e is a SAED pattern of β phase along $[\overline{345}]_d$ zone axis. $[\overline{345}]$ direction of the disordered phase is corresponding to $[01\bar{1}]_\beta$ direction of β phase. Fig. 5f is a simulated electron diffraction pattern along $[01\bar{1}]_\beta$ zone axis, which is consistent with the experimental pattern in Fig. 5e. The above results point out that the structural model of β phase is correct.

For the structural model of γ phase, the analysis is similar to that of β phase. The first step is to gain the ordered unit, as shown in Fig. 6a. The second step is to determine the value of n. The stacking sequence (ABCABC...) of FCC structure causes that n is 3N, where N is a positive integer. For a V layer in Fig. 6a, the proportion of ordered structural vacancies is 1/4. If n is assumed to the minimum value 3, stacking sequence along $[\bar{1}11]$ direction will be VBCVBC... and p will be 1/12, which will be lower than p_0. When n is assumed to be 3N, p is equal to 1/12N. For simplicity, n is considered to be three. The possible structural model of γ phase shown in Fig. 6b is obtained by the space group $P3m1$ with the lattice parameters $a_\gamma = b_\gamma = \sqrt{2}a$, $c_\gamma = \sqrt{3}a$, $\alpha_\gamma = \beta_\gamma = 90°$, $\gamma_\gamma = 120°$.

Fig. 6c and Fig. 6d are a simulated electron diffraction pattern and a HRTEM image, which are consistent with the experimental FFT image (Fig. 4b) and HRTEM image (Fig. 4a), respectively. It should be noticed that half of structural vacancies in γ phase are still disordered. As previously mentioned, the superstructure spots (e.g., 1/6{422}) of γ phase are hard to be observed

in SAED patterns. For the same season, HRTEM images of γ phase along other zone axes are also hard to be obtained. We will continue studying γ phase by TEM and other methods in the future.

4.3 Formation mechanism of β and γ phases

For β and γ phases, a question is raised that which phase appears first during disorder-order phase transformation. As discussed in Section 4.2, the structural vacancies in β and γ phase are fully and partially ordered, respectively. As the phase transformation goes on, the order degree increases. Thus，γ phase appears first and then turns into β phase. Furthermore, in view of energy minimization, the transformation sequence is also reasonable. For β phase, ordered structural vacancies in V layers are the nearest neighbors to one another. For γ phase, ordered structural vacancies in V layers are separated by an atom. The theory about combination forms of tri-vacancy [43] shows that, comparing with that in γ phase, the arrangement of vacancies in β phase is more stable and its bonding is preferred. This finding can explain that the probability of occurrence of 1/3{422} spots is much higher than that of 1/6{422} spots.

The formation mechanism of β and γ phases is proposed based on the above discussion and the formation mechanism of negative Frank dislocation-loop [44] in FCC structure. The driving force and resistance of ordering process are the mixing energy parameter E_m and the entropy of configuration, respectively [45]. When the system is cooled, thermal vibrations of Hg and In atoms are weakened and then structural vacancies with high concentration tend to group and form preferentially vacancy discs along {111} planes with the minimal surface energy. Before the formation of vacancy discs, there is a transition state with high-energy, i.e. γ phase.

The formation process of the two phases can be divided into four processes, as shown in Fig. 7. Hg, In and structural vacancies are expressed by dots in red, yellow and blue, respectively. The

{111} planes are expressed by A, B and C layers. The four processes are as follows: (1) In Fig. 7a，Hg, In and structural vacancies are distributed randomly at cation sublattice. From Fig. 7a to Fig. 7b, when phase transformation begins, a number of atoms in A layers move to the positions of structural vacancies and left structural vacancies at original positions. Accordingly, structural vacancies gather in A layers and then form a transition state (γ phase) with relatively low energy. (2) From Fig. 7b to Fig. 7c, when phase transformation goes on, atoms in A layers keep on moving to the positions of structural vacancies nearby and vacancy discs with lower energy start to form. For satisfying the percentage of 1/6, vacancy discs tend to be distributed with the interval of five {111} planes and to form β-phase nucleus. (3) From Fig. 7c to Fig. 7d, atoms, near both sides of vacancy discs, keep on moving to the positions of structural vacancies far away. The vacancy discs begin to become bigger and β phases grow. (4) As indicated in Fig. 7e, when the sizes exceed a critical value, the vacancy discs collapse and decrease the lattice constants of β phases. It should be stressed that a Frank dislocation-loop will form on two sides of a vacancy disc. The dislocation theory shows that the Frank dislocation loop cannot slip. Accordingly, the vacancy disc also cannot slip. Thereby, β phase is relatively stable and is easy to be observed.

5. Conclusions

$Hg_3In_2Te_6$ (MIT) crystals grown by Bridgman method are studied by high-resolution transmission electron microscopy (HRTEM). The results show that the crystals contain ordered phase domains, indicating disorder-order phase transformation still happens in the portions of ingots, which cannot be observed in XRD spectra. The low thermal conductivity of the MIT disordered phase promoted the transformation.

Two new types of ordered phases (β and γ phases) exist in some areas of MIT crystals.

Possible atomic models of the two superstructures are suggested based on HRTEM images: (1) β phase in the structure $P3m1$ with $a_\beta = b_\beta = \sqrt{2}a/2$, $c_\beta = 2\sqrt{3}a$; (2) γ phase in the structure $P3m1$ with $a_\gamma = b_\gamma = \sqrt{2}a$, $c_\gamma = \sqrt{3}a$. The structural vacancies of β phase are entirely ordered and that of γ phase are partially ordered with the order degree of 1/2.

A mechanism is proposed to explain the formation and evolution of the two ordered phases. When disorder-order phase transformation starts, part of structural vacancies gather along some {111} planes and then form γ phases. Afterward, structural vacancies keep on gathering along {111} planes and form β-phase nuclei. With the development of phase transformation, vacancy discs become bigger and β phases grow. When the sizes exceed a critical value, the vacancy discs collapse and decrease lattice constants of β phases.

Acknowledgements

The authors thank beneficial discussion and valuable advice with Dr. Maosen Fu. This work has been financially supported by the National "973" Program (2011CB610406), the National Natural Science Foundation of China (Grant No. 51202197, 51172185), the 111 Project of China (Grant No. B08040). It is also supported by the Specialized Research Fund for the Doctoral Program of Higher Education of China (20116102120014), the Natural Science Basic Research Plan in Shaanxi Province of China and the Fund of Ministry of Education for Doctor (20116102110013).

Reference

1. A. I. Malik, M. Vieira, M. Fernandes, F. Macarico and Z. M. Grushka, *SPIE*, 1999, 3629, 433-442.
2. C. A. Maynell, G. A. Saunders and T. Seddon, *Phys. Lett.*, 1970, 23, 338-339.
3. D. C. Papadopoulos and C. Manolikas, *Mater. Res. Bull.*, 2000, 35, 359-367.

4. L. H. Wang, W. Q. Jie, Y. Yang and L. Fu, *J. Phys. D-Appl. Phys.*, 2008, 41, 085411-085414.
5. O. L. Maslyanchuk, L. A. Kosyachenko, German, II, I. M. Rarenko, V. A. Gnatyuk and T. Aoki, *Phys. Status Solidi C* 2009, 6, 1154-1157.
6. L. A. Kosyachenko, I. S. Kabanova, V. M. Sklyarchuk, O. F. Sklyarchuk and I. M. Rarenko, *Phys. Status Solidi A*, 2009, 206, 351-355.
7. A. Gomyo, T. Suzuki, K. Kobayashi, S. Kawata, I. Hino and T. Yuasa, *Appl. Phys. Lett.* , 1987, 50, 673-675.
8. K. Kurosaki, H. Matsumoto, A. Charoenphakdee, S. Yamanaka, M. Ishimaru and Y. Hirotsu, *Appl. Phys. Lett.* , 2008, 93, 012101-012103.
9. K. Ken and Y. Shinsuke, in *Modules, Systems, and Applications in Thermoelectrics*, CRC Press, 2012, DOI: 10.1201/b11892-10, pp. 1-9.
10. L. H. Wang, W. Q. Jie, G. Q. Zha and G. Xu, *Mater. Sci. Eng. B*, 2006, 133, 129-131.
11. L. H. Wang, W. Q. Jie and Y. Yang, *Mater. Sci. Eng. B*, 2008, 150, 2-5.
12. L. H. Wang and W. Q. Jie, *J. Cryst. Growth*, 2006, 290, 203-206.
13. L. G. Wang, Y. C. Dong and W. Q. He, *Mater. Res. Bull.*, 2007, 42, 1949-1954.
14. L. H. Wang, Y. C. Dong and W. Q. Jie, *J. Phys. D-Appl. Phys.*, 2007, 40, 3921-3924.
15. L. Wang and W. Jie, *J. Cryst. Growth*, 2013, 362, 327-329.
16. L. Wang, Doctor of Engineering, Northwestern Polytechnical University, 2008.
17. C.-e. Kim, K. Kurosaki, M. Ishimaru, D.-y. Jung, H. Muta and S. Yamanaka, *Phys. Status Solidi RRL*, 2009, 3, 221-223.
18. C.-e. Kim, K. Kurosaki, M. Ishimaru, H. Muta and S. Yamanaka, *Journal of Elec Materi*, 2011, 40, 999-1004.
19. S. Yamanaka, M. Ishimaru, A. Charoenphakdee, H. Matsumoto and K. Kurosaki, *Journal of Elec Materi*, 2009, 38, 1392-1396.
20. L. Kienle, V. Duppel, A. Simon and H. J. Deiseroth, *Z. Anorg. Allg. Chem.*, 2003, 629, 1412-1420.
21. T. Plirdpring, K. Kurosaki, A. Kosuga, M. Ishimaru, A. Harnwunggmoung, T. Sugahara, Y. Ohishi, H. Muta and S. Yamanaka, *Appl. Phys. Lett.* , 2011, 98, 172104-3.
22. P. Spencer, *Br. J. Appl. Phys.* , 1964, 15, 625-632.
23. K. Durose, in *CdTe and Related Compounds; Physics, Defects, Hetero-and Nano-structures, Crystal Growth, Surfaces and Applications: Physics, CdTe-based Nanostructures, Semimagnetic Semiconductors, Defects*, 2009, pp. 174-175.
24. Y. Pei and D. T. Morelli, *Appl. Phys. Lett.* , 2009, 94, 122112-122113.
25. G. Li, S.-J. Shih, Y. Huang, T. Wang and W. Jie, *J. Cryst. Growth*, 2008, 311, 85-89.
26. G. Yang, A. E. Bolotnikov, Y. Cui, G. S. Camarda, A. Hossain, K. H. Kim, J. Franc, E. Belas and R. B. James, *Journal of Elec Materi*, 2013, 42, 3138-3141.
27. L. P. Tan, T. Sun, S. Fan, R. V. Ramanujan and H. H. Hng, *J. Alloys Compd.* , 2014, 587, 420-427.
28. M. Nie, J. Zhang, F. Huang, J. W. Liu, X. K. Zhu, Z. L. Chen and L. Z. Ouyang, *J. Alloys Compd.* , 2014, 588, 348-356.
29. T. Karakostas and N. A. Economou, *Phys. Status Solidi A*, 1975, 31, 89-99.
30. M. Guymont, A. Tomas, M. P. Pardo and M. Guittard, *Phys. Status Solidi A*, 1989, 113, K5-K7.
31. A. Tomas, M. Guymont, M. P. Pardo, M. Guittard and J. Flahaut, *Phys. Status Solidi A*, 1988, 107, 775-784.
32. N. Teraguchi, F. Kato, M. Konagai, K. Takahashi, Y. Nakamura and N. Otsuka, *Appl. Phys. Lett.* , 1991, 59, 567-569.

33. C. Manolikas, *Phys. Status Solidi A*, 1982, 69, 393-405.
34. T. Okamoto, M. Konagai, N. Kojima, A. Yamada, K. Takahashi, Y. Nakamura and O. Nittono, *Journal of Elec Materi*, 1993, 22, 229-232.
35. T. Okamoto, N. Kojima, A. Yamada, M. Konagai, K. Takahashi, Y. Nakamura and O. Nittono, *Jpn. J. Appl. Phys.*, 1992, 31, L143-L144.
36. G. L. Bleris, T. Karakostas, N. A. Economou and R. de Ridder, *Phys. Status Solidi A*, 1978, 50, 579-586.
37. Z. R. Dai and F. S. Ohuchi, *Appl. Phys. Lett.* , 1998, 73, 966-968.
38. S. S. Shankar, A. Rai, B. Ankamwar, A. Singh, A. Ahmad and M. Sastry, *Nat. Mater.* , 2004, 3, 482-488.
39. J. C. Heyraud and J. J. Métois, *Surf. Sci.* , 1980, 100, 519-528.
40. Y. Sun, B. Mayers and Y. Xia, *Adv. Mater.* , 2003, 15, 641-646.
41. Y. Sun, B. Mayers and Y. Xia, *Nano Lett.* , 2003, 3, 675-679.
42. V. Germain, J. Li, D. Ingert, Z. L. Wang and M. P. Pileni, *J. Phys. Chem. B*, 2003, 107, 8717-8720.
43. A. C. Damask and G. J. Dienes, *Point defects in metals*, Gordon and Breach, New York, 1963.
44. J. P. Hirth and J. Lothe, *Theory of dislocations*, John Wiley & Sons, Inc., New York, 1982.
45. J. Pan, J. Tong and M. Tian, *Foundation of Material Science*, Tsinghua University Press, Bejing, 2011.

Figure captions

Fig. 1 Typical powder XRD pattern, HRTEM image and FFT image obtained from MIT samples: (a) powder XRD pattern; (b) HRTEM image; (c) FFT image.

Fig. 2 HRTEM image and the results of β ordered phase: (a) HRTEM image; (b) FFT image; (c) schematic diagram of (b); (d) schematic diagram of (a); (e) order unit of (d). The indices marked are corresponding to the structure of the disordered phase.

Fig. 3 Selected area electron diffraction (SAED) pattern of β ordered phase along [$\bar{1}11$] zone axis of the disordered phase. The indices marked are corresponding to the structure of the disordered phase. The inset is an enlarged image of Fig. 3.

Fig. 4 HRTEM image and the results of γ ordered phase: (a) HRTEM image; (b) FFT image; (c) schematic diagram of (b); (d) schematic diagram of (a); (e) order unit of (d). White dots in (a) are expressed by blue dots in (d) and (e).

Fig. 5 Structural model, simulated and experimental results of β phase: (a) ordered unit; (b) structural model; (c) simulated electron diffraction pattern along [$\bar{1}11$]$_d$ zone axis; (d) simulated HRTEM image along [$\bar{1}11$]$_d$ zone axis; (e) experimental SAED pattern along [$\bar{3}\bar{4}5$]$_d$ zone axis; (f) simulated electron diffraction pattern along $[01\bar{1}]_\beta$ zone axis. For clear observation, Te atoms are not represented. The subscripts d and β represent the disordered phase and β phase, respectively.

Fig. 6 Structural model, simulated results of γ phase: (a) ordered unit; (b) structural model; (c) simulated electron diffraction pattern along [$\bar{1}11$]$_d$ zone axis; (d) simulated HRTEM image along [$\bar{1}11$]$_d$ zone axis.

Fig. 7 Schematic diagrams of the formation mechanism of β and γ phases. It should be emphasized that the migration paths of Hg and In atoms are only schematic diagrams and practical paths are complicated.

Tab. 1 Comparison of interplanar distances along <422> directions in Fig. 1, 2 and 4.

Figures	symbol	<422>/nm	$<24\bar{2}>$/nm	$<2\bar{2}4>$/nm	Mean value/nm	Multiple of d
Fig.1b	d	0.129	0.129	0.128	0.129	1
Fig.2a	D_1	0.376	0.381	0.375	0.377	2.92
Fig.4a	D_2	0.733	0.734	0.729	0.732	5.67

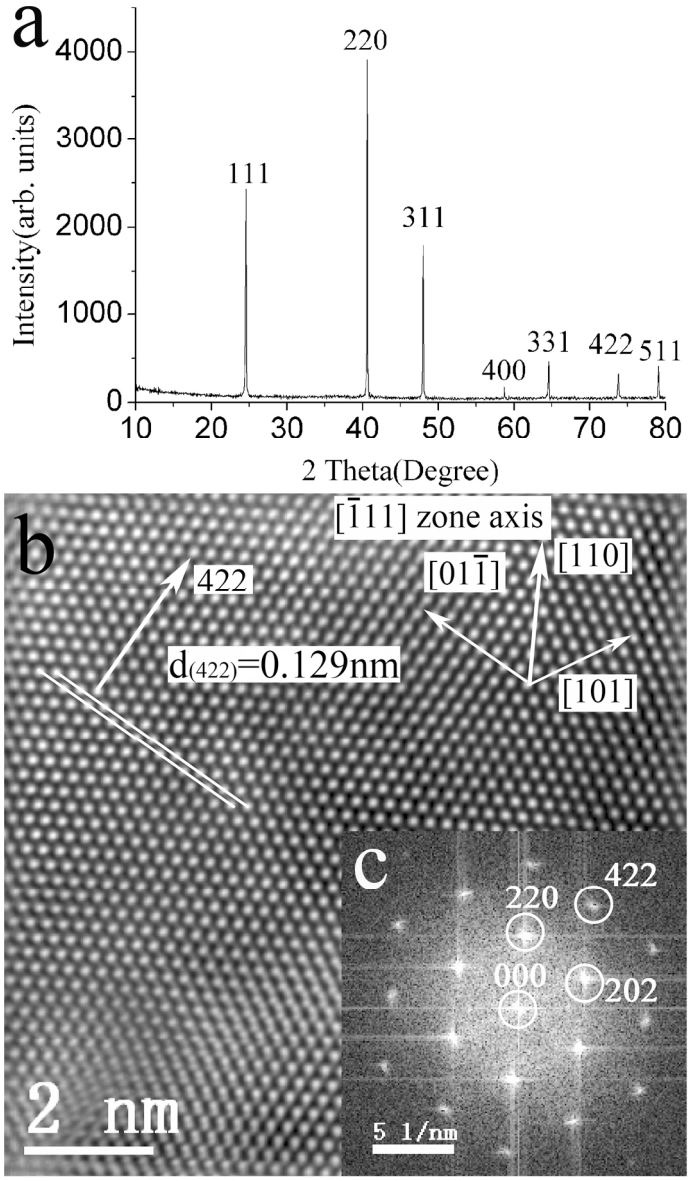

Fig. 1 Typical powder XRD pattern, HRTEM image and FFT image obtained from MIT samples: (a) powder XRD pattern; (b) HRTEM image; (c) FFT image.
147x255mm (300 x 300 DPI)

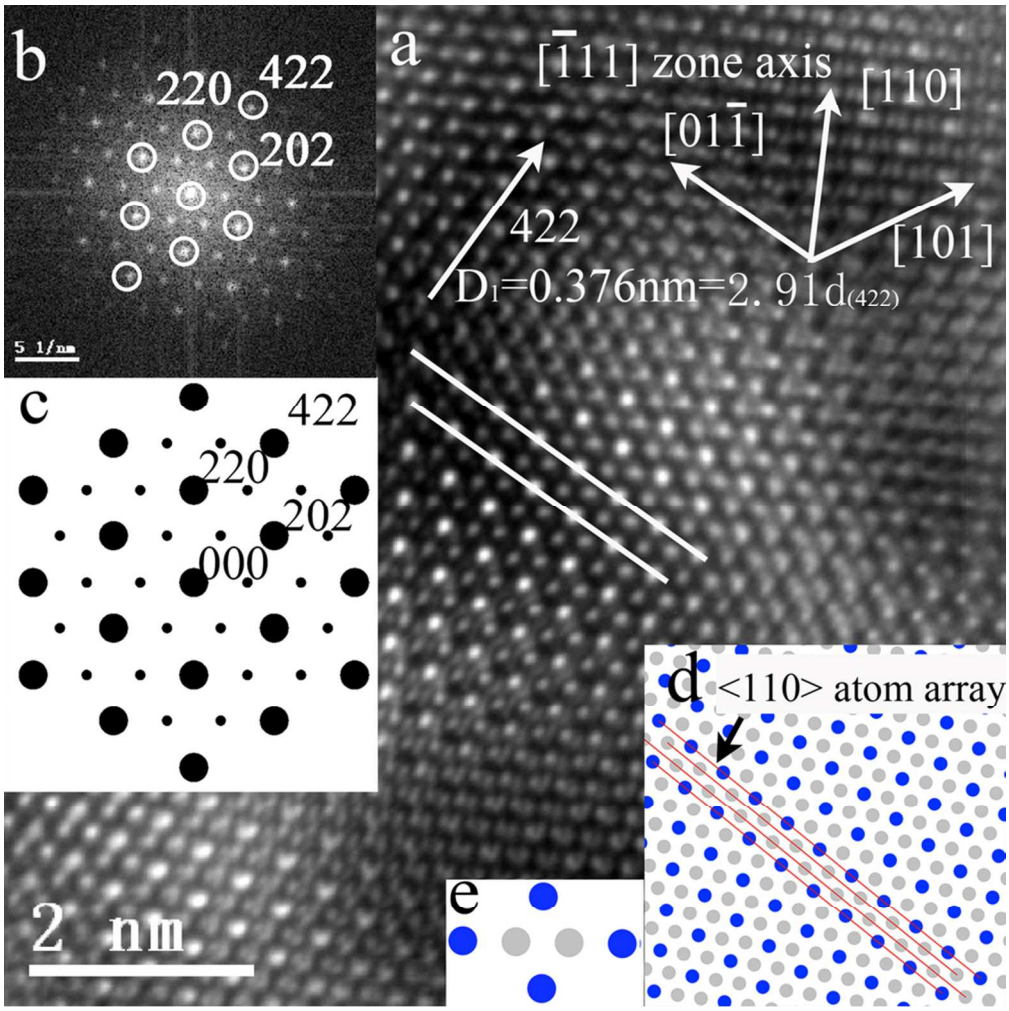

Fig. 2 HRTEM image and the results of β ordered phase: (a) HRTEM image; (b) FFT image; (c) schematic diagram of (b); (d) schematic diagram of (a); (e) order unit of (d). The indices marked are corresponding to the structure of the disordered phase.
85x85mm (300 x 300 DPI)

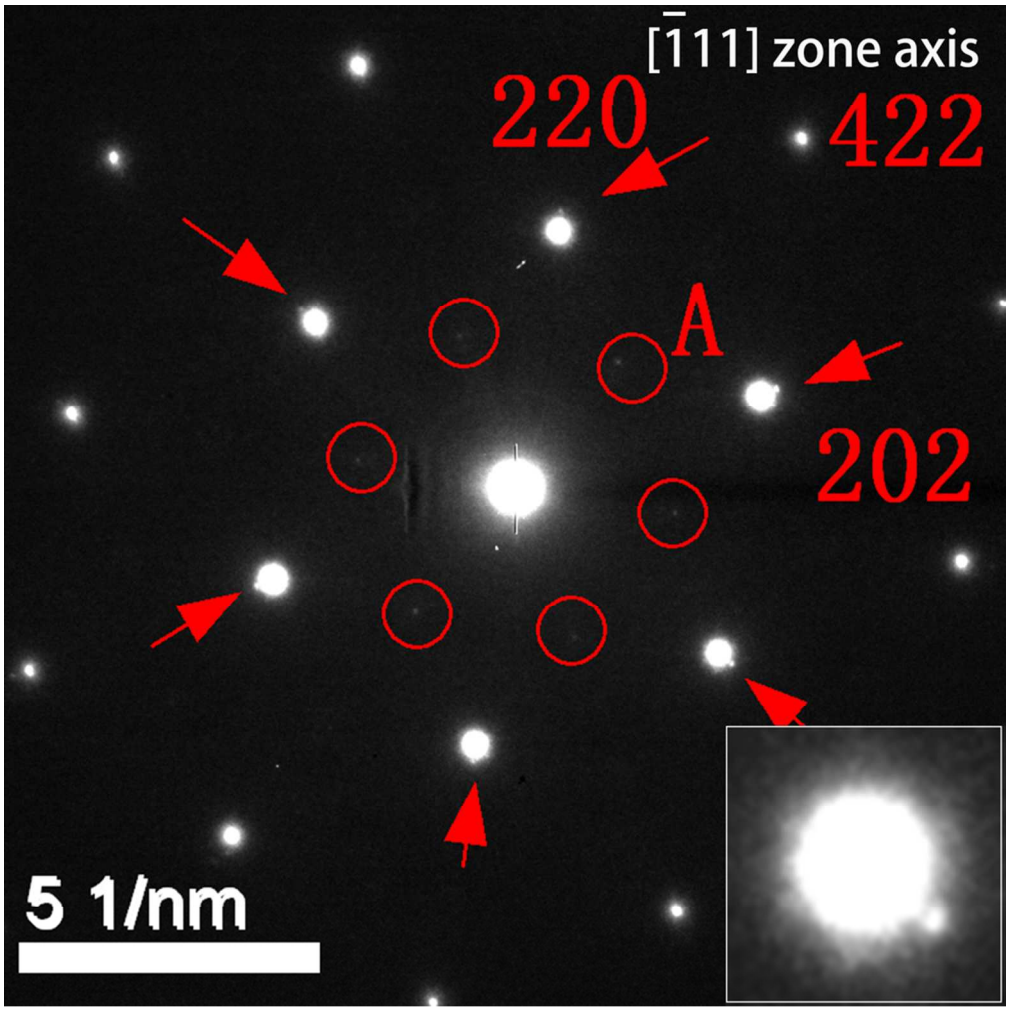

Fig. 3 Selected area electron diffraction (SAED) pattern of β ordered phase along [-111] zone axis of the disordered phase. The indices marked are corresponding to the structure of the disordered phase. The inset is an enlarged image of Fig. 3.
85x85mm (300 x 300 DPI)

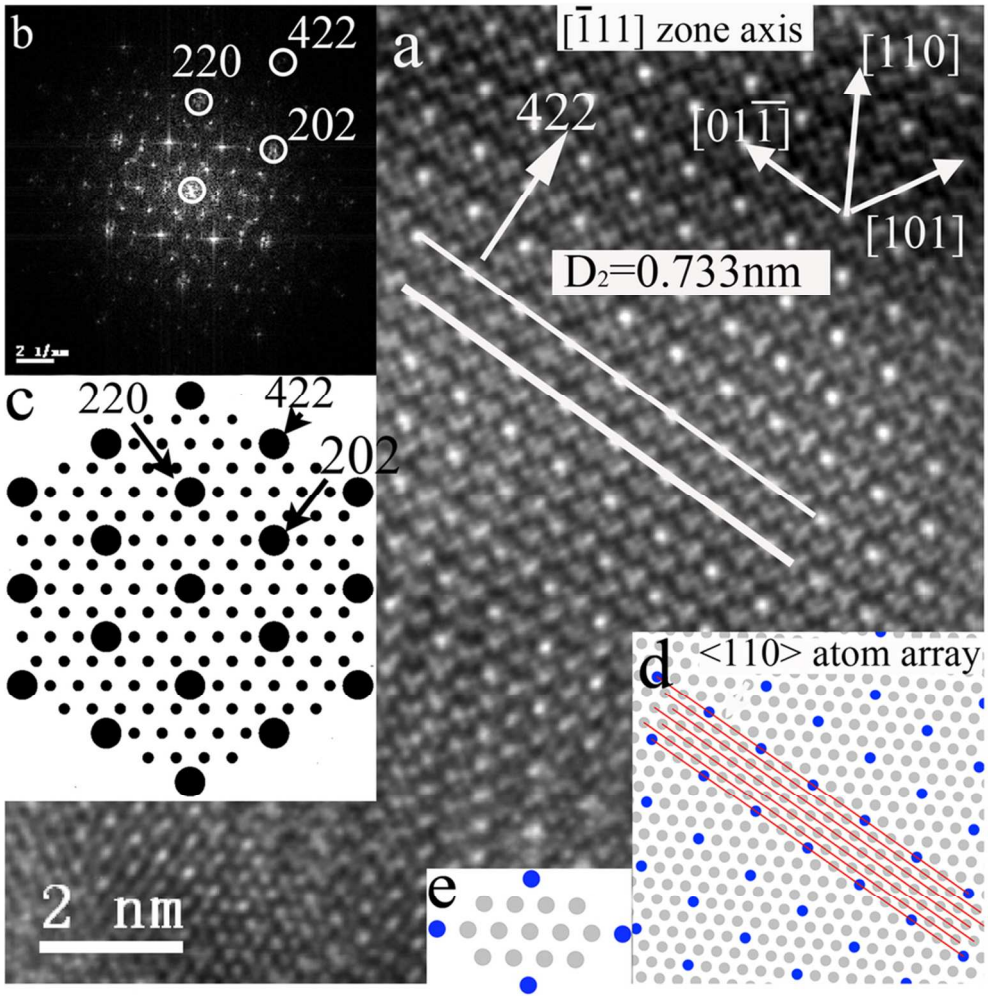

Fig. 4 HRTEM image and the results of γ ordered phase: (a) HRTEM image; (b) FFT image; (c) schematic diagram of (b); (d) schematic diagram of (a); (e) order unit of (d). White dots in (a) are expressed by blue dots in (d) and (e).
85x85mm (300 x 300 DPI)

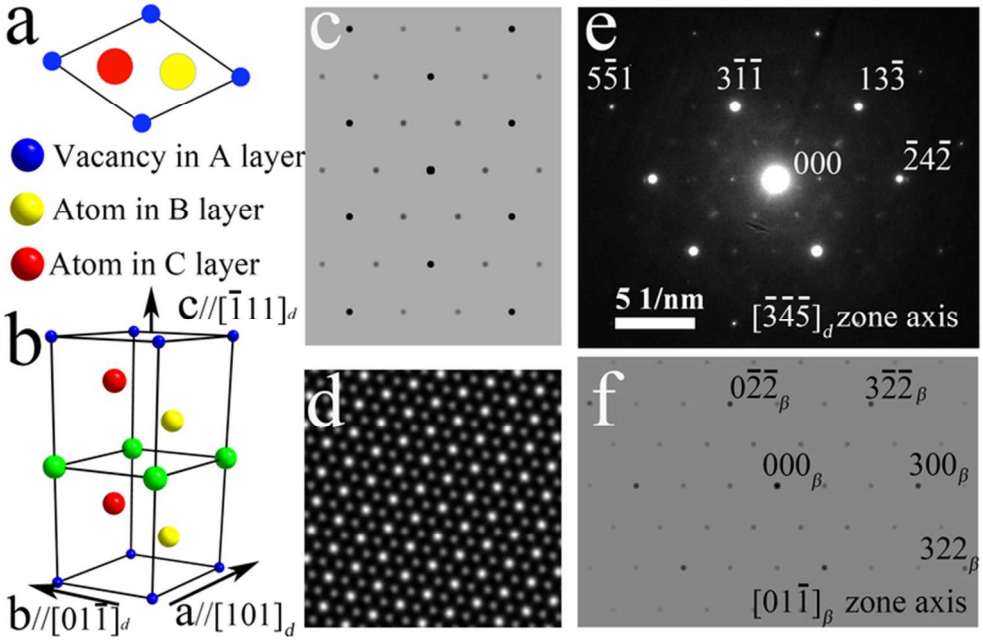

Fig. 5 Structural model, simulated and experimental results of β phase: (a) ordered unit; (b) structural model; (c) simulated electron diffraction pattern along $[-111]_d$ zone axis; (d) simulated HRTEM image along $[-111]_d$ zone axis; (e) experimental SAED pattern along $[-3-4-5]_d$ zone axis; (f) simulated electron diffraction pattern along $[01-1]_\beta$ zone axis. For clear observation, Te atoms are not represented. The subscripts d and β represent the disordered phase and β phase, respectively.
69x44mm (300 x 300 DPI)

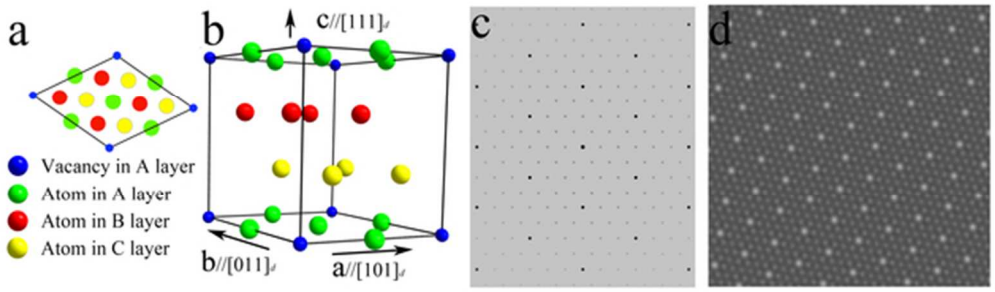

Fig. 6 Structural model, simulated results of γ phase: (a) ordered unit; (b) structural model; (c) simulated electron diffraction pattern along $[-111]_d$ zone axis; (d) simulated HRTEM image along $[-111]_d$ zone axis.
53x16mm (300 x 300 DPI)

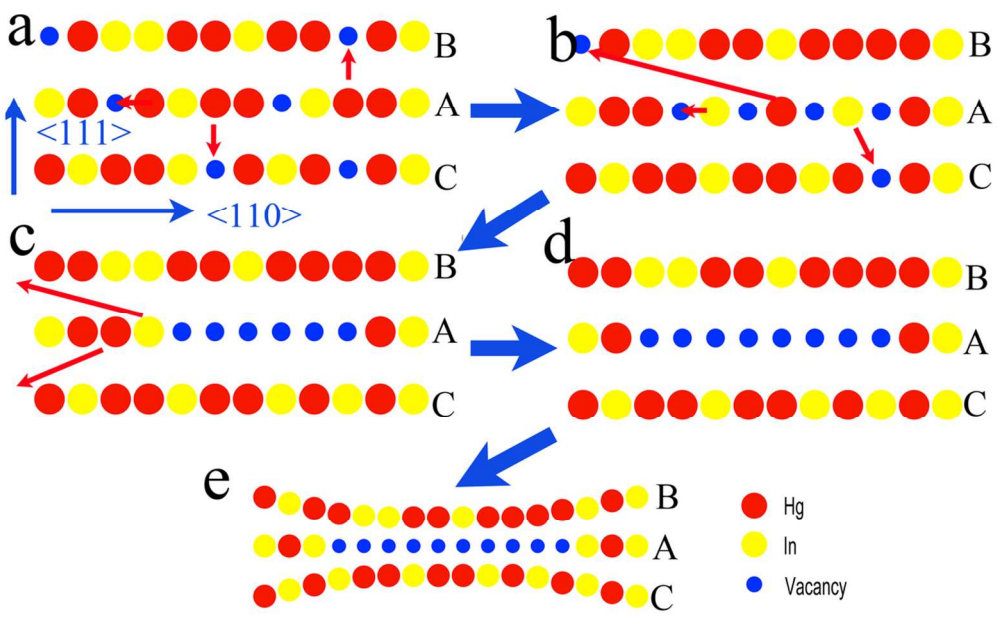

Fig. 7 Schematic diagrams of the formation mechanism of β and γ phases. It should be emphasized that the migration paths of Hg and In atoms are only schematic diagrams and practical paths are complicated.
55x34mm (600 x 600 DPI)

A table of contents entry

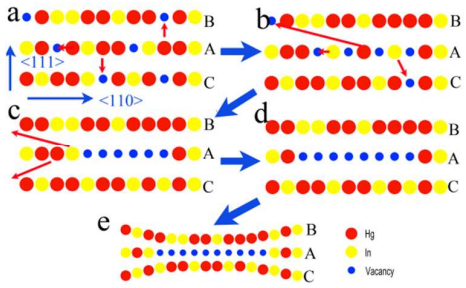

The formation and the evolution of two $Hg_3In_2Te_6$ phases with ordered vacancies during the disorder-order transformation process.